# Coil-in-Coil Carbon Nanocoils: 11 Gram-Scale Synthesis, Single Nanocoil Electrical Properties, and Electrical Contact Improvement

**Nujiang Tang,[†,*] Waston Kuo,[‡,§,*] Chienchung Jeng,[‡,§] Liyuan Wang,[‡] Kuanjiuh Lin,[∥] and Youwei Du[†]**

[†]Department of Physics and Nanjing National Laboratory of Microstructures, Nanjing University, Nanjing 210093, PR China, [‡]Department of Physics, [§]Institute of Nanoscience, and [∥]Department of Chemistry and Center of Nanoscience and Nanotechnology, National Chung Hsing University, Taichung, 402, Republic of China

**ABSTRACT** Coil-in-coil carbon nanocoils (CNCs) were synthesized by means of acetylene decomposition using nickel nanoparticles as catalysts. The investigations revealed that there are often several CNCs self-assembled in one nanospring. The yield of coil-in-coil CNCs was high up to 11 g in each run at the decomposition temperature of 450 °C. CNC nanodevices were fabricated for systematical examinations of charge conduction in the single CNC and in the electrical contacts. A focused laser beam of about 70 μm in diameter was applied for selective annealing CNC nanodevices so as to improve the electrical contacts to the CNC. Our study showed that the selective focused laser annealing technique is an effective route to improve the electrical contacts to the nanodevice. Temperature-dependent CNC resistances are analyzed with the Mott-variable range hopping (VRH) and Efros—Shklovskii VRH model, revealing electron hopping conduction in the disordered CNCs with a characteristic length of about 5—50 nm.

**KEYWORDS:** carbon nanocoils · coiled structures · catalytic growth · electrical property · electrical contact improvement

Since carbon coils were discovered by Davis *et al.* in 1953,[1] they have stirred great interests due to potential applications in micromagnetic sensors, mechanical microsprings or actuators, high elastic electro-conductors, high electromagnetic waves absorber, electro-magnetic (EM) nano-transformers, and wearable electronics, *etc.*[2−9] Up to now, various properties of carbon coils such as mechanical,[6] field emission,[10] EM wave absorption,[11] thermal[12] and electric[13] properties, and so forth have been studied. Especially, the EM and electrical properties have aroused special interest. For example, the electrical properties of carbon microcoils (CMCs)/silicone-rubber composites on the changes in the values of electrical parameters as a function of CMCs content in the matrix were measured using an impedance analyzer in the frequency range of 40−200 kHz; and percolation paths were observed at a CMC content of 3 wt %.[13] The capacitance with a small value was dominant at CMC content less than 3 wt %, and the resistance was dominant at CMC content higher than 3 wt %. Only a 1−2 wt % addition of CMCs in PMMA beads resulted in strong EM wave absorption; however, an addition of CMCs greater than 5 wt % resulted in decrease of EM absorption.[14] The temperature dependence (in the range of 5−300 K) of the electric resistance and magnetoresistance (MR) of as-prepared and annealed CMCs were measured.[15] The as-prepared CMCs show no MR, while the CMCs annealed at temperatures higher than 2500 °C show negative MR of −3.5% at 5 K under the magnetic field of 5 T but positive MR of 1% at 300 K under the magnetic field of 5 T. The dependence of MR on calcination temperature may attribute to the difference of carrier concentration resulted in graphitization. The field direction dependence of the MR shows that the current flows helically along the fiber constituting the CMCs. Shen *et al.*[16] measured the electrical properties of a single CMC with a double helix structure by a standard four-probe technique. Their study revealed that the temperature dependence of the resistance above 13 K is in accordance with Mott−David variable range hopping, whereas below 13 K, it is in accordance with Efros−Shklovskii variable range hopping. In addition, a positive MR with $H^2$-dependence behavior is observed at low temperature. Recently, Chiu *et al.*[17] measured the transport properties in a single carbon coil from ambient temperature to 64 mK. The temperature-dependent resistance was analyzed with the Efros−Shklovskii variable range hopping model, indicating three-dimensional electron hopping conduction in the disordered

*Address correspondence to tangnujiang@nju.edu.cn, wkuo@phys.nchu.edu.tw

Received for review October 14, 2009 and accepted January 12, 2010.

**Published online January 21, 2010.** 10.1021/nn901417z

carbon coils with a characteristic length of about 5 nm. A CMCs sample was evaluated for use as a microsolenoid in a small magnetic device.[18] A direct current was supplied to the single CMC and a micro/nanomagnetic field generated from the coil was observed directly by means of electron holography. A computer simulation of electron holography was also done to analyze the magnetic field quantitatively.

Moreover, nanodevices based on single semiconducting nanowires have received much attention because of potential applications in nanoscaled electronics. Of particular interest are carbon nanotubes[19] and graphene layers[20] due to their unique electron band structures, and from which p−n junction diodes and field effect transistors have been demonstrated at the room temperature. However, metal/semiconductor nanocontacts of the nanowire devices are usually of high resistances so as to bring in drawbacks in device performance and reliability. For instance, the measured contact resistance of carbon nanotubes ranges from kΩ to MΩ at room temperature according to literature. Usually people account this deviation in different Schottky barrier heights to various work functions of the contact metal.[21] Moreover, poor contacts may result from the barriers formed at the contact interface due to surface contamination or oxidation of the nanomaterials in prior to contact fabrication. Nevertheless one is possible to obtain Ohmic metal/nanowire contacts by choosing suitable contact metals[22,23] and applying appropriate soldering[24] or annealing.[25,26] Nowadays the rapid thermal annealing (RTA), widely used for fast heating samples of large area, has been a key step in increasing the performance of nanowire-based transistors.[26] Among the RTA methods, the laser annealing, having potential advantages of not only a shorter annealing time but also a smaller annealing area, will be an important technique in nanodevice fabrications worthy of further studies. For example, ultrafast annealing has been tried by using pulsed lasers in semiconducting nanowires for activating implanted dopants[27] and in nanoparticle synthesis for reducing the particle size[28−31] as well as nanowelding them together.[32]

Up to now, carbon nanocoil (CNC) materials were commonly produced by combustion chemical vapor deposition (CCVD) of carbon source gases, for example, acetylene and ethylene over metal catalysts such as Fe, Ni, Cu, *etc*. It is notable that the mass production of high pure CNCs still remains a large challenge. We reported previously the synthesis of T-CNCs[33] and plait-like CNCs[34] with high yield, the yields of each run are *ca*. 3.027 and 3.705 g, respectively. Herein, we reported the preparation of CNCs showing a novel coil-in-coil structure, and the yield of each run is high up to *ca*. 11 g. Furthermore, nanodevices based on single CNC were fabricated and from which the electrical properties of single CNC were investigated. The conduction mechanism is identified as three-dimensional electron hopping with electron−electron interaction. Especially in our CNCs the electrons have robust Coulomb interaction with Coulomb gaps ranging from several MeV to 20 MeV. Finally, we introduced a selective focused laser annealing technique, which is an effective route to improve the electrical contacts to the nanodevice. For receiving the benefits of high anneal temperatures, small and controllable anneal areas and *in-situ* electrical measurement, it is an ideal route for single-nanowire devices.

## RESULTS AND DISCUSSION

**Microstructures of the as-Prepared Sample.** The catalytic precursor powder was measured by X-ray fluorescence spectrometer. The result showed that the content of halide ions is *ca*. 15.43033 wt %, indicating the content of $NiCl_2$ is 28.19 wt %. Namely, the catalytic precursors include nickel oxide and $NiCl_2$. Notable, our previous work showed that the catalytic precursor can be reduced to metallic nickel, and highly pure Ni catalyst can be obtained after the catalytic precursor was reduced in $H_2$ at the temperatures of ≥375 °C.[33,35] By using 0.163 g catalytic precursor powder as a catalyst precursor, 11 g CNCs was obtained in each run by CVD of acetylene at 450 °C. As compared to a yield of 2.41 g obtained using 51 mg of nickel oxide at 425 °C[33] and 3.032 g obtained using 25 mg of nickel oxide at 415 °C,[34] there is a significant increase in the yield of each run upon using a larger quantity of the catalyst at higher temperature. This result can be confirmed by thermogravimetric-differential thermal analysis (TG-DTA). As shown in Figure 1a, the weight loss of 98.34% in the as-prepared sample, as the temperature increased from 450−700 °C. The leftover powder of only 1.66 wt % can be attributed to the NiO powder. This result indicates that the Ni nanoparticles, prepared through hydrogen reduction using the sol-gel method, reveal high catalytic performance at the relatively low temperature of 450 °C. This low-temperature CVD approach might be viable in the mass production for future application of CNCs. Moreover, the diffraction peaks in the X-ray diffraction (XRD) pattern (Figure 1b) of the as-prepared CNCs can be related to typical phases ($d_{(002)}$ = 0.34 nm; $d_{(101)}$ = 0.204 nm) of graphite structure, indicating that the formation of the graphite results from the complete decomposition of acetylene. Finally, Raman studies offered further information on the possible characteristics of the graphite structure. The Raman spectrum (Figure 1c) of the as-prepared sample exhibits two peaks at *ca*. 1355.79 and 1592.02 $cm^{-1}$ with approximately equal intensity. Since crystalline graphites (such as highly oriented pyrolitic graphite) show a characteristic Raman peak at 1580 $cm^{-1}$ (called G-band), and carbon materials with disordered structures give an intense "defect-induced" band at 1350 $cm^{-1}$ (called D-band).[11] In the as-prepared CNCs, the appearance of D-band and the broader half-width

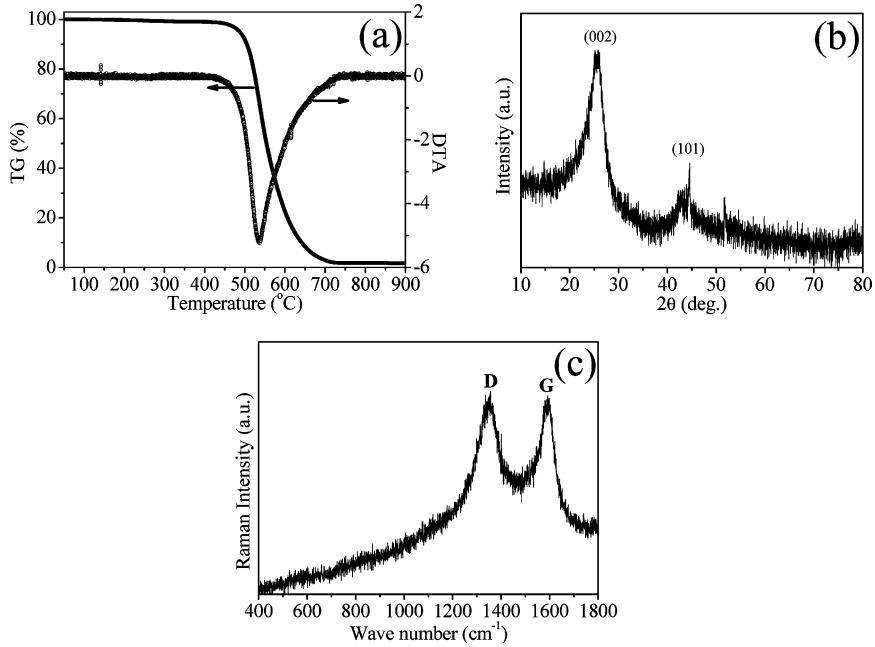


**Figure 1. Characterization of the as-prepared CNCs: (a) TG-DTA curves in air, (b) XRD pattern, (c) Raman spectrum.**

(67.6 $cm^{-1}$) are evidence for the presence of disorder and/or distortion in the sample.

The morphologies of the as-prepared CNCs have also been examined through field-emission scanning electron microscopy (FE-SEM) and transmission electron microscopy (TEM). The FE-SEM image (Figure 2a) reveals that the sample obtained is CNCs with springlike structure and high purity. The diameters of CNCs range from 120 to 500 nm, and their lengths are often more than 30 μm, significantly bigger and longer than the CNCs that we previously reported.[33,34] Furthermore, the TEM image (Figure 2b) clearly shows that most CNCs are coiled in a regular and tight fashion with short pitch. Showing in Figure 2c is a typical CNC which was ruptured after being agitated in an ultrasonic bath; it demonstrated that the coils contain many small fibers with the diameter of *ca.* 5 nm. The structure of springlike coil-in-coil CNCs is similar to T-CNCs[33] reported before where the coils are composed of bundles of nanofibers of *ca.* 10 nm in diameter. The difference in fabrication procedure is that in the case of springlike CNCs, 163 mg of the catalytic precursor powder was spread on a ceramic plate which was placed inside a quartz reaction tube (diameter, 5.2 cm; length, 85 cm) (see Experimental Section), whereas in the case of T-CNCs, 51 mg of the catalytic precursor powder was spread on a ceramic plate (which was placed the quartz reaction tube) was placed in a stainless steel tube of 5.2 cm inner diameter. The structure of spring-like CNCs is different from that of plait-like CNCs[34] where two CNCs of different handiness form an interangle of 0°. It is apparent that the growth mechanism of carbon nanomaterials is complex and subject to subtle changes of reaction conditions.

Figure 3 is the variations of the yield of CNCs in each run as a function of temperature of acetylene decomposition. It showed that the decomposition temperature has profound influence on the yield of carbon products. At 400 °C, there is a low yield of 0.173 g. The yield reaches the maximum value of 11 g at 450 °C. Above 450 °C, with the increase of the decomposition temperatures, the yield decreases. Above 500 °C, the yield decreases very fast. The yield decreases to only 0.6 g at the decomposition temperature of 650 °C. The results show that with the use of the Ni catalysts prepared by this method, the temperature of 450 °C is most suited to the growth of the CNCs.

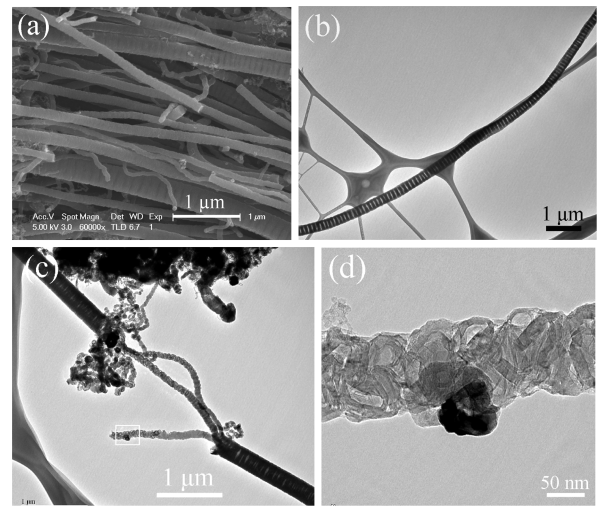


**Figure 2. Microstructure of the sample. (a) FE-SEM image. (b, c, and d) TEM images: (c) CNC which was ruptured after being agitated in an ultrasonic bath; (d) magnified image of the corresponding position marked in panel c.**

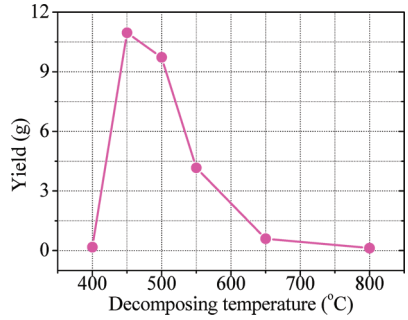


**Figure 3. The variations of the yield of CNCs in each run as a function of temperature of acetylene decomposition.**

**Electrical Properties of the Single CNCs and Electrical Contact Improvement.** Figure 4a is a SEM image of a CNC nanodevice, in which multiple 300 nm-wide Cr/Au electrodes with thickness of 50 nm/140 nm are arranged with an edge-to-edge spacing of 300 nm on a 110 nm-in-diameter CNC. By using 2-terminal and 3-terminal measurements,[24] we can estimate the contact resistances of devices successfully made. To understand the quality of the nano-contacts to the CNCs, we analyzed 100 contacts in 20 devices successfully made and divided them into several groups according to their contact resistance. Figure 4b is the frequency distribution of contact resistances of un-annealed samples at room temperature. We note that no clear electrode-material (Ti or Cr) dependence was found in this analysis. One can see that the resistance distribution ranges in orders of magnitude from $10^4$ Ω to $10^9$ Ω, and one-forth of the contacts are significantly poor (resistance higher than 100 MΩ). Such poor contacts usually have rapidly increasing resistances as temperature decreases so as to hinder the transport measurements at lower temperatures. Therefore, the devices with poor contacts required annealing treatment for improving the electrical contacts before undergoing further low temperature measurements.

The best annealing condition can reduce the contact resistances from hundreds MΩ to *ca.* 100 kΩ, a reduction of 3 orders of magnitude. Before employing further studies, we carefully checked all the 2, 3, and 4-terminal resistances as well as the SEM images of the devices after the annealing process and excluded any that showed unexpected changes in resistance and morphology. Especially, the 4-terminal resistances of the devices show almost the same value despite that 2-terminal or 3-terminal resistances reduce dramatically in the annealing treatment. It reveals that most of the CNCs show a high specific resistance of 15−45 Ω/nm under 4-terminal measurements at the room temperature.

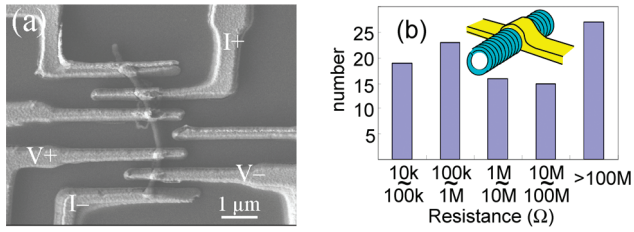


**Figure 4. (a) The SEM image of a CNC nanodevice. The configuration of the 4-terminal measurement presented in Figure 9 are indicated. (b) The frequency distribution of contact resistances of as-prepared samples at room temperature. Inset depicts how the metallic electrodes contact to the CNC.**

The temperature dependence of the CNC resistance and contact resistance can provide us more information about the charge conduction in the CNC and the contact region. A closed cycle cryogenic system is employed for our need, cooling the samples from room temperature down to 10 K. As illustrated in Figure 5a, the current-voltage (*IV*) characteristic of an annealed sample A1 becomes nonlinear at lower temperatures in the bias-voltage range of several mV. The nonlinearity is best presented in Figure 5b, in which the dynamical conductance ($G_d$ = d*I*/d*V*) *versus* bias-voltage curve at 10 K shows a dip in the vicinity of zero-bias voltage.

A closer inspection reveals that the current follows a power law that $I(V) \propto V^{\eta}$ in a large range of bias voltage from several mV to 100 mV. Figure 6 is the log−log plot of the *IV* curves of the annealed sample A1 at low temperatures of 10, 20, and 40 K, respectively. One can clearly see a kink around 10 mV: At smaller bias-voltages, the *IV* is found to be more linear while at larger bias, it follows a power law $I(V) \propto V^{\eta}$. When *T* is lower than 50 K, the nonlinearity starts to grow up and η increases as *T* decreases, reaching the value of 1.6 at $T = 10$ K. However, the *IV* curves behave more linear at smaller bias voltages of about several mV, and the slope in the *IV* curve saturates to the inverse of zero-bias resistance.

The zero-bias resistance may reflect the charge conduction of the CNC in the equilibrium state. For instance, that of the A1 CNC increases from about 70 kΩ at 300 K to 2.5 MΩ at 10 K, and the temperature dependence can be best fit to the following expression,

$$R(T) = R_0 \exp\left[\left(\frac{T_0}{T}\right)^{1/d}\right] \qquad (1)$$

with $d = 4$ in the high temperature regime ($T > 20$ K), whereas in the low temperature regime ($T < 20$ K), $d = 2$. For disordered semiconductors, $d = 4$ dependence can be explained by Mott variable range hopping (VRH) of (non-interacting) localized electrons, while $d = 2$ by Efros−Shklovskii (E−S) VRH model, a signature of robust Coulomb interaction between the electrons. This property of sample A1 was also further confirmed by cooling the sample down to 2 K (see data A1* in Table 1). Obviously the resistance is distinct after several thermal cycles but the value of *d* is unchanged. For samples without laser annealing treatment, the CNC resistances also show similar temperature dependence (*e.g.*, U3 data shown in Figure 7a). We note that the VRH behavior has been observed in helical carbon fibers of 150 nm[21] and several μm in diameter.[20] From the result, and

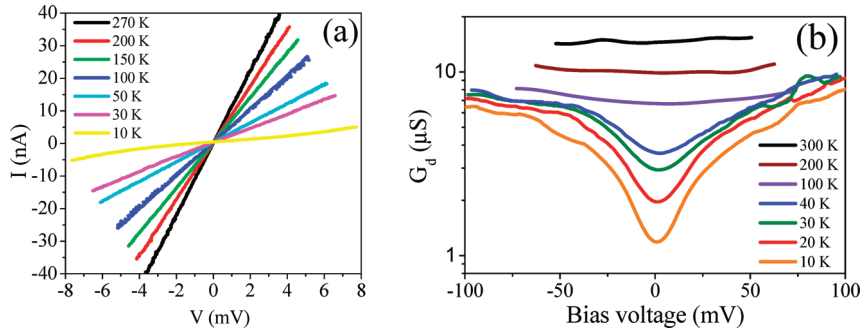


**Figure 5. (a) Four-terminal *IV* curves of annealed sample A1, at various temperatures ranging from 270 to 10 K. (b) The differential conductance as a function of bias voltage with a large bias range at various temperatures from 300 to 10 K.**

a high specific resistance for most of the CNCs measured at the room temperature, we conclude that these CNCs are highly disordered because of the presence of disorder and/or distortion in the sample (Figure 1c), and the electrons conduct through localized states so as to exhibit a crossover from Mott to E−S VRH[36] from 300 to 2 K. This finding is consistent with the knowledge that the graphene $sp^2$ lattice structure cannot form coiled structure without large number of atomic defects, such as 5-membered and 7-membered rings in the materials.[4] Moreover, the E−S VRH is also confirmed in the non-linear *IV* curve at low temperatures, signifying the formation of a Coulomb gap.

To unambiguous determine the important parameters governing the Mott-to-E−S VRH, various works demonstrated a universal crossover scaling form for temperature-dependent resistance.[37,38] Among them a simple scaling form of $\log(R/R_0) \propto f(T/T_x)$ with $f(x) = 1 + x^{-1}((1 + x)^{1/2} - 1)/[(1 + x)^{1/2} - 1]^{1/2}$ has been suggested by Aharony *et al.*[37] At high temperatures ($T \gg T_x$), the $d = 4$ dependence is recovered, whereas at low temperatures ($T \ll T_x$), the $d = 2$ result is obtained. Here $T_x$ is the crossover temperature. Indeed, our data can be well scaled to the universal function $f(x)$ as shown in Figure 8, a strong support of the observation of Mott-to-E−S VRH. From the curve fitting, we determined for sample A1 the characteristic Mott temperature, $T_M$ to be about 2080 K and the characteristic Efros−Shklovskii temperature, $T_{ES}$, to be about 168 K. From the microscopic point of view, we note that the Mott temperature gives $N(E_F)l^3 = 100$ eV$^{-1}$, in which $l$ is the localization length and $N(E_F)$ is the density of state (DOS) at Fermi energy $E_F$. In contrast, the E−S VRH originates from the Coulomb interaction and yields $\kappa l = 3.5$ μm with a dielectric constant κ. Because our CNC diameters are on the order of 100 nm, the above analysis would be valid only if dielectric constant has a lower limit of 50. Considering the charge screening effect from localized electrons, one may have $\kappa \approx 1 + 4\pi e^2 N(E_F) l^2/\varepsilon_0$, and the enhancement in κ is possible. To find out the localization length, one needs the information of the DOS, $N(E_F)$, which have been reported from $10^{19}$ to $10^{21}$ (eV$^{-1}$ cm$^{-3}$) in previous works. On the basis of the above analysis and an assumption that DOS of our CNC is similar to those have been reported, we estimate our localization length is in the range of 4.6−22 nm, a reasonable value for a 3-dimensional hopping in our CNCs with 110 nm in diameter. In turn, the dielectric constant is further determined as on the order of $10^2$ to $10^3$, a much smaller value than that in ref 21 but still fulfilling previous assumptions. The Coulomb

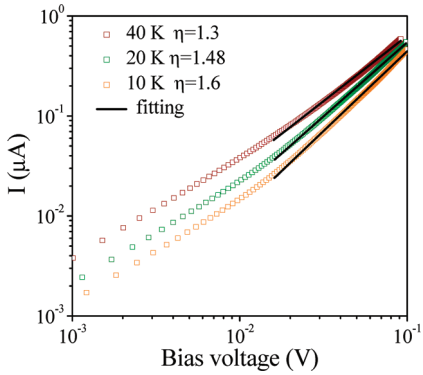


**Figure 6. The annealed sample A1 clearly shows power-law dependent *IV* curves in the log−log plot at low temperatures of 10, 20, and 40 K, respectively.**

**TABLE 1. A Comparison of the Electronic Properties of the Carbon Coils Reported to Date**

| sample description | Shen, J. Y. *et al.* ref 16 | Chiu, H. S. *et al.* ref 17 | U3 (without laser annealing) | A1 (300 s laser annealed) | A1* (A1 with 2-300 K thermal cycle) |
|---|---|---|---|---|---|
| coil diameter | ~2 μm | ~150 nm | ~150 nm | ~110 nm | ~110 nm |
| $T_M$ (K) | 2342 | N/A | 215 | 2080 | 227 |
| $T_{ES}$ (K) | 17.5 | 0.17 | 272 | 168 | 160 |
| $N(E_F)$ (eV$^{-1}$ cm$^{-3}$) | ~$10^{19}$ | $4.4 \times 10^{20}$ | N/A | N/A | N/A |
| $l$ (nm) | 13.2 | 32 | 11−50 | 4.6−22 | 9.7−45 |
| κ | ~$10^3$ | ~$10^6$ | 50−200 | 150−750 | 70−350 |
| Coulomb gap (MeV) | 0.12 | $1.5 \times 10^{-3}$ | 23.8 | 3.7 | 10.5 |

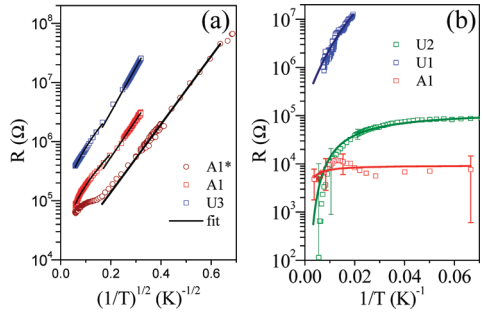


**Figure 7. (a) Four-terminal resistances as a function of $T^{-1/2}$ of annealed sample A1, and un-annealed sample U3. Data A1* are those of the sample A1 after several thermal cycles from 2 K to room temperature. The solid curves are fit to the expression (1) with $d = 4$ on the high temperature side and with $d = 2$ on the low temperature side. (b) The contact resistance as a function of $T^{-1}$ of un-annealed samples A1, U1, and U2. The solid curves are fit to the thermal fluctuation-induced tunneling model described in text.**

gap due to charge interaction can be obtained as about 3.7 MeV for A1 and 23.8 MeV for U3 through the formula, $U \approx e^3(N(E_F)/\kappa^3\varepsilon_0^3)^{1/2} \approx 0.905 k_B T_{ES}^{3/2} T_M^{-1/2}$. The Coulomb gaps in our CNCs are greatly larger than those of carbon coils reported to date, implying much weaker charge screening effects in these CNCs. As such excitons may have a large binding energy in these CNCs, an interesting topic for future studies as that have been reported in single-walled carbon nanotubes.[39] Some important parameters mentioned above can be found in Table 1 for a summary.

We may also investigate the temperature dependence of the single contact resistance as shown in Figure 7b obtained by subtracting a 2-terminal resistance by 3-terminal resistance. Because the data are obtained by subtracting 2-terminal resistance with 3-terminal one, relative error becomes large when the contact resistance is much small than 3-terminal resistance. Remarkably the contact resistance of annealed sample A1, by accounting experimental errors, is almost independent to the temperature. Notice that the contact of U2, although having a smaller resistance than that of A1 at room temperature, increases rapidly and surpasses at the temperature of 100 K because of the flat temperature dependence of the A1 contact. Actually more data has been acquired but not enough for quantitatively getting single contact resistance. Nevertheless in general we found 2-terminal and 3-terminal resistances of annealed samples have much weaker temperature dependences than those of un-annealed samples. At high temperatures $T > 50$ K, the temperature-dependent contact resistances roughly obey the thermal activation behavior of a Schottky-type contact in which $R(T) \propto \exp(\Phi/k_BT)$ with a barrier height $\Phi$.[40] However, a closer inspection reveals that some contact resistances saturate at very low temperature. We believe that, as reported in the contacts of $RuO_2$ nanowires,[41] this kind of contacts have quantum tunneling features at low temperatures and can be explained by the thermal fluctuation-induced tunneling.[42] The data can well be fit to the expression suggested by Sheng *et al.*,[42]

$$R(T) = R_0 \exp\left(\frac{T_1}{T + T_0}\right) \qquad (2)$$

In this expression the resistance follows a thermal-activation result at high temperatures, whereas it saturates to a value featuring quantum tunneling through the barrier at lower temperatures. Assuming a contact area of about 200 nm × 100 nm and an electron mass similar to that in free space, one can obtain the barrier widths in annealed sample A1 contact as roughly 10 nm and the barrier heights as tens of MeV. However, the barrier area cannot be judged by microscopy images and might be smaller than expected, leading to thinner but higher barriers. The barrier width of the U2 contact is larger than that of annealed sample A1 contact because of the stronger temperature dependence and a higher saturation resistance. From the observations above, we conclude that despite strong disorder in the CNCs, the disorder originated from the contact region can be reduced after the appropriate laser annealing.

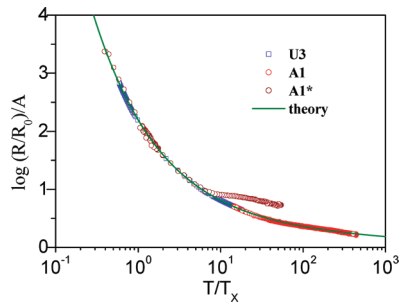


**Figure 8. The scaling plot for the Mott-to-E−S crossover for the three curves shown in Figure 7a. The data can be well-scaled to a function $f(T/T_x)$ described in the text.**

## CONCLUSIONS

In summary, we provide a favorable route for 11 g-scale production of springlike CNCs with novel coil-in-coil structure by the pyrolysis of acetylene at 450 °C over Ni nanoparticles, and no carrier gas such as argon and nitrogen was needed. Thus, we have provided a simple, low-cost, and environmentally friendly approach for the mass production of springlike CNCs. By regulating the temperature for acetylene pyrolysis, one can control the CNC yield. The study of the charge conduction in the single CNC and in the electrical contacts showed the electrons hop from and to localized states with a characteristic length of about 5−50 nm due to strong disorder in the CNCs. At lower temperatures, the electron−electron interaction in the localized state forms a soft Coulomb gap of several meV, turning the electron hopping into an Efros−Shklovskii VRH form. On the contact resistance, the Schottky-type are often observed at high temperatures while annealed contacts show pronounce quantum tunneling at low temperatures. The well-monitored and controlled annealing

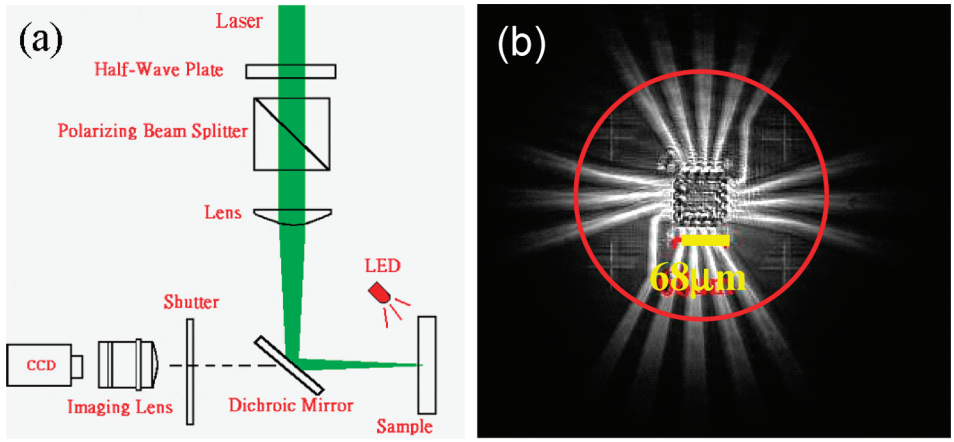


**Figure 9. (a) The schematic for laser annealing setup. (b) The charge-coupled device image clearly shows the luminous spot, marked by the red circle, of diameter of 300 μm on the sample. By further focus, the spot can be reduced to about 70 μm in diameter, but hardly resolved by the CCD camera.**

process successfully reduces the resistances of the metallic contacts for strongly disordered CNCs, and the contact resistance as a function of temperature is flat, suggesting thinner barrier for electron conduction in the contact region. We envision the selective laser annealing integrated by automatic positioning stage will be a powerful tool in the near future for productions of nanowire-based transistors.

## EXPERIMENTAL SECTION

**Experimental Procedure.** In our synthesis, a preparative procedure similar to those of the T-CNCs[33] and plait-like CNCs[34] was used to prepare the CNCs materials. $NiCl_2 \cdot 6H_2O$ (0.03 mol) and citric acid (0.045 mol) monohydrate were well mixed and stirred for 4 h in 100 mL of absolute ethanol at 60 °C. After that, ethanol was evaporated at 80 °C and the resulting residual xerogel was heated at 400 °C in air for 4 h to yield a catalytic precursor powder. A 0.163 g portion of the catalytic precursor powder was spread on a ceramic plate. The plate was then placed inside a reaction tube (a quartz tube 5.3 cm in diameter and 85 cm in length, equipped with temperature and gas-flow controls). The catalytic precursor powder was reduced with a $H_2$ flow at 450 °C for 3 h. After turning off the $H_2$ flow, a stream of acetylene was introduced. Then acetylene was pyrolyzed at 450 °C for 1 h at atmospheric pressure over the reduced nickel nanoparticles. After the system was cooled to room temperature, approximately 11 g of "as-prepared" CNCs was obtained.

**Characterization of the Samples.** The phases of the samples were determined by XRD with Cu Kα radiation (model D/Max-RA, Rigaku, Japan) at room temperature. Raman spectroscopic investigation of the samples was performed using a Jobin-Yvon LA-BRAM HR800 instrument with 514.5 nm Ar laser excitation. The morphologies of the samples were examined by TEM (model JEM-2100, Japan), and FE-SEM (model JSM-6700F, Japan) with the equipment operated at an accelerating voltage of 200 and 5 kV, respectively. For TEM analysis, the powder samples were dispersed in ethanol, agitated in an ultrasonic bath, and finally deposited on a copper grid that was coated with a carbon film.

**Fabrications of CNC Nanodevices.** For CNC nanodevice fabrication, substrates were diced from silicon wafers coated with 300 nm-thick $SiO_2$ or $Si_3N_4$ insulating layers on which micrometer-sized metal pads and alignment marks are made by using standard photolithography. The CNCs were first dispersed in alcohol, prepared for random dripping on the substrates using a micropipet. For further confining the area for CNC deposition, a windowed photoresist as a blocking layer was coated on the substrates before the dripping. CNCs being spread on the blocking layer would be removed from the substrates and then dipped in the resist remover. We note that the resist window can also serve as a sieve for the CNCs according to the window size. When the CNC deposition was done, the positions of the selected CNCs were carefully determined by the SEM images and were then used for designing the submicrometric electrical leads. Ti/Au and Cr/Au electrodes were then patterned using e-beam lithography and were placed on the top of the selected CNCs by thermal evaporation and followed by the lift-off process. Because of the springlike structure, the outer diameter of the CNC can be as large as 100 nm, and a thick metal deposition is needed for a good crossover.

**Laser Annealing of CNC Nanodevices.** As shown in Figure 9a, we employed a continuous doubled Yb:YAG laser (of wavelength = 515 nm), and the laser beam goes through a half-wave plate and a polarizing beam splitter for a rapid change of the power, finally delivering a power of about 4 W on the samples. The beam spot is about 300 μm in diameter as illustrated in the image captured by a charge-coupled device (CCD) camera (Figure 9b) and can be reduced to 70 μm with further focusing. By mounting the sample on a 2-axis *XY* moving stage and wire-bonding it to electrical measurement instruments, we are able to control precisely the beam spot position and area on the substrate as well as trace the resistance *in situ*.

*Acknowledgment.* The authors acknowledge the assistance in low temperature measurement from Y. W. Suen at NCHU and C. S. Wu at NCUE. We are also grateful for fruitful discussions with C. D. Chen, J. J. Lin, J. P. Bird, and Y. Ochiai. This work was supported by the National Major Project of Fundamental Research: Nanomaterials and Nanostructures (2005CB623605 and 2010CB923402), P. R. China, and the National Science Council of Taiwan (NSC96-2112-M-005-003-MY3) and Center of Nanosicence and Nanotechnology, NCHU.

## REFERENCES AND NOTES

1. Davis, W. R.; Slawson, R. J.; Rigby, G. R. Unusual Form of Carbon. *Nature* **1953**, *171*, 756.
2. Iijima, S.; Toshinary, I.; Ando, Y. Pentagons, Heptagons and Negative Curvature in Graphite Microtubule Growth. *Nature* **1992**, *356*, 776–778.
3. Amelinckx, S.; Zhang, X. B.; Bernaerts, D.; Zhang, X. F.; Ivanov, V.; Nagy, J. B. A Formation Mechanism for Catalytically Grown Helix-Shaped Graphite Nanotubes. *Science* **1994**, *265*, 635–639.
4. Akagi, K.; Tamura, R.; Tsukada, M.; Itoh, S.; Ihara, S. Electronic Structure of Helically Coiled Cage of Graphitic Carbon. *Phys. Rev. Lett.* **1995**, *74*, 2307–2310.

5. Volodin, A.; Ahlskog, M.; Seynaeve, E.; Haesendonck, C. Van; Fonseca, A.; Nagy, J. B. Imaging the Elastic Properties of Coiled Carbon Nanotubes with Atomic Force Microscopy. *Phys. Rev. Lett.* **2000**, *84*, 3342–3345.
6. Chen, X.; Zhang, S.; Dikin, D. A.; Ding, W.; Ruoff, R. S.; Pan, L.; Nakayama, Y. Mechanics of a Carbon Nanocoil. *Nano Lett.* **2003**, *3*, 1299–1304.
7. Alexandre, F. d. F.; Douglas, S. G. Mechanical Properties of Nanosprings. *Phys. Rev. Lett.* **2004**, *92*, 175502.
8. Varadan, V. K.; Varadan, V. V. Electromagnetic Shielding and Absorptive Materials. U.S. Patent No. 89/03890 (1989).
9. Bajpai, V.; Dai, L. M.; Ohashi, T. Large-Scale Synthesis of Perpendicularly Aligned Helical Carbon Nanotubes. *J. Am. Chem. Soc.* **2004**, *126*, 5070–5071.
10. Pan, L. J.; Hayashida, T.; Zhang, M.; Nakayama, Y. Field Emission Properties of Carbon Tubule Nanocoils. *Jpn. J. Appl. Phys.* **2001**, *40*, L235–L237.
11. Chen, X.; Motojima, S.; Iwanaga, H. Carbon Coatings on Carbon Microcoils by Pyrolysis of Methane and Their Properties. *Carbon* **1999**, *37*, 1825–1831.
12. Shibagaki, K.; Motojima, S. Thermal Behavior and Effect of Heat Treatment in an Inert Gas on Oxidized Carbon Microcoils. *Carbon* **2001**, *39*, 411–417.
13. Katsuno, T.; Chen, X.; Yang, S.; Motojima, S.; Homma, M.; Maeno, T.; Konyo, M. Observation and Analysis of Percolation Behavior in Carbon Microcoils/Silicone-Rubber Composite Sheets. *Appl. Phys. Lett.* **2006**, *88*, 232115.
14. Motojima, S.; Hoshiya, S.; Hishikawa, Y. Electromagnetic Wave Absorption Properties of Carbon Microcoils/PMMA Composite Beads in W Bands. *Carbon* **2003**, *41*, 2658–2660.
15. Fujii, M.; Matsui, M.; Motojima, S.; Hishikawa, Y. Magnetoresistance in Carbon Microcoils Annealed at Various Temperatures. *J. Cryst. Growth* **2002**, *237*, 1937–1941.
16. Shen, J. Y.; Chen, Z. J.; Wang, N. L.; Li, W.; Chen, L. Electrical Properties of a Single Microcoiled Carbon Fiber. *Appl. Phys. Lett.* **2006**, *89*, 153132.
17. Chiu, H. S.; Lin, P. I.; Wu, H. C.; Hsieh, W. H.; Chen, C. D.; Chen, Y. T. Electron Hopping Conduction in Highly Disordered Carbon Coils. *Carbon* **2008**, *47*, 1761.
18. Yamamoto, K.; Hirayama, T.; Kusunoki, M.; Yang, S. M.; Motojima, S. Electron Holographic Observation of Micromagnetic Fields Current-Generated from Single Carbon Coil. *Ultramicroscopy* **2006**, *106*, 314–319.
19. Tans, S. J.; Verschueren, A. R. M.; Dekker, C. Room-Temperature Transistor Based on Single Carbon Nanotubes. *Nature* **1998**, *393*, 49–52.
20. Novoselov, K. S.; Geim, A. K.; Morozov, S. V.; Jiang, D.; Zhang, Y.; Dubonos, S. V.; Grigorieva, I. V.; Firsov, A. A. Electric Field Effect in Atomically Thin Carbon Films. *Science* **2004**, *306*, 666–669.
21. Leonard, F.; Talin, A. A. Size-Dependent Effects on Electrical Contacts to Nanotubes and Nanowires. *Phys. Rev. Lett.* **2006**, *97*, 026804.
22. Lin, Y. C.; Lu, K. C.; Wu, W. W.; Bai, J.; Chen, L. J.; Tu, K. N.; Huang, Y. Single Crystalline PtSi Nanowires, PtSi/Si/PtSi Nanowire Heterostructures, and Nanodevices. *Nano Lett.* **2008**, *8*, 913–918.
23. Chen, Z.; Appenzeller, J.; Knoch, J.; Lin, Y. M.; Avouris, P. The Role of Metal-Nanotube Contact in the Performance of Carbon Nanotube Field-Effect Transistors. *Nano Lett.* **2005**, *5*, 1497–1502.
24. Hsiou, Y. F.; Yang, Y. J.; Stobinski, L.; Kuo, W.; Chen, C. D. Controlled Placement and Electrical Contact Properties of Individual Multiwalled Carbon Nanotubes on Patterned Silicon Chips. *Appl. Phys. Lett.* **2004**, *84*, 984–986.
25. Bachtold, A.; Henny, M.; Terrier, C.; Strunk, C.; Schönenberger, C.; Salvetat, J. P.; Bonard, J. M.; Forró, L. Contacting Carbon Nanotubes Selectively with Low-Ohmic Contacts for Four-Probe Electric Measurements. *Appl. Phys. Lett.* **1998**, *73*, 274–276.
26. Derycke, V.; Martel, R.; Appenzeller, J.; Avouris, P. Controlling Doping and Carrier Injection in Carbon Nanotube Transistors. *Appl. Phys. Lett.* **2002**, *80*, 2773–2775.
27. Cui, Y.; Zhong, Z.; Wang, D.; Wang, W. U.; Lieber, C. M. High Performance Silicon Nanowire Field Effect Transistors. *Nano Lett.* **2003**, *3*, 149–152.
28. Ok, Y. W.; Seong, T. Y.; Choi, C. J.; Tu, K. N. Field Emission from Ni-Disilicide Nanorods Formed by Using Implantation of Ni in Si Coupled with Laser Annealing. *Appl. Phys. Lett.* **2006**, *88*, 043106.
29. Misra, N.; Xu, L.; Pan, Y.; Cheung, N. Excimer Laser Annealing of Silicon Nanowires. *Appl. Phys. Lett.* **2007**, *90*, 111111.
30. Kamat, P. V.; Flumiani, M.; Hartland, G. V. Picosecond Pynamics of Silver Nanoclusters. Photoejection of Electrons and Fragmentation. *J. Phys. Chem. B* **1998**, *102*, 3123–3128.
31. Takami, A.; Kurita, H.; Koda, S. Laser-Induced Size Reduction of Noble Metal Particles. *J. Phys. Chem. B* **1999**, *103*, 1226–1232.
32. Fujiwara, H.; Yanagida, S.; Kamat, P. V. Visible Laser Induced Fusion and Fragmentation of Thionicotinamide-Capped Gold Nanoparticles. *J. Phys. Chem. B* **1999**, *103*, 2589–2591.
33. Tang, N. J.; Zhong, W.; Au, C. T.; Yang, Y.; Han, M. G.; Lin, K. J.; Du, Y. W. Synthesis, Microwave Electromagnetic, and Microwave Absorption Properties of Twin Carbon Nanocoils. *J. Phys. Chem. C* **2008**, *112*, 19316–19323.
34. Tang, N. J.; Yang, Y.; Lin, K. J.; Zhong, W.; Du, Y. W. Synthesis of Plait-like Carbon Nanocoils in Ultrahigh Yield, and Their Microwave Absorption Properties. *J. Phys. Chem. C* **2008**, *112*, 10061–10067.
35. Tang, N. J.; Zhong, W.; Liu, W.; Jiang, H. Y.; Du, Y. W. Synthesis and Complex Permeability of Ni/$SiO_2$ Nanocomposite. *Nanotechnology* **2004**, *15*, 1756–1758.
36. Zhang, Y.; Dai, O.; Levy, M.; Sarachik, M. P. Probing the Coulomb Gap in Insulating n-Type CdSe. *Phys. Rev. Lett.* **1990**, *64*, 2687.
37. Aharony, A.; Zhang, Y.; Sarachik, M. P. Universal Crossover in Variable Range Hopping with Coulomb Interactions. *Phys. Rev. Lett.* **1992**, *68*, 3900.
38. Meir, Y. Universal Crossover between Efros−Shklovskii and Mott Variable-Range-Hopping Regimes. *Phys. Rev. Lett.* **1996**, *77*, 5265.
39. Wang, F.; Cho, D. J.; Kessler, B.; Deslippe, J.; Schuck, P. J.; Louie, S. G.; Zettl, A.; Heinz, T. F.; Shen, Y. R. Observation of Excitons in One-Dimensional Metallic Single-Walled Carbon Nanotubes. *Phys. Rev. Lett.* **2007**, *99*, 227401.
40. Card, H. C.; Rhoderick, E. H. Studies of Tunnel Mos Diodes. 1. Interface Effects in Silicon Schottky Diodes. *J. Phys. D: Appl. Phys.* **1971**, *4*, 1589.
41. Lin, Y. H.; Chiu, S. P.; Lin, J. J. Thermal Fluctuation-Induced Tunneling Conduction through Metal Nanowire Contacts. *Nanotechnology* **2008**, *19*, 365201.
42. Sheng, P.; Sichel, E. K.; Gittleman, J. I. Fluctuation-Induced Tunneling Conduction in Carbon−Polyvinylchloride Composites. *Phys. Rev. Lett.* **1978**, *40*, 1197–1200.